Non-destructive Measurement of the Charge Transfer Across $LaMnO_3/SrTiO_3$ Interfaces

Shohei Miyagawa[1], Yuta Ishii[2], Masato Anada[1,3], Kazuki Nagai[1,3], Miho Kitamura[4], Hiroshi Kumigashira[5], and Yusuke Wakabayashi[1a]

[1] *Department of Physics, Graduate School of Science, Tohoku University, Sendai 980-8578, Japan*

[2] *National Institute for Materials Science, Center for Basic Research on Materials (CBRM), 1-2-1 Sengen, Tsukuba, Ibaraki 305-0003, Japan*

[3] *Division of Materials Physics, Graduate School of Engineering Science, Osaka University, Toyonaka 560-8531, Japan*

[4] *National Institutes for Quantum Science and Technology (QST), Sendai, 980-8579, Japan*

[5] *Institute of Multidisciplinary Research for Advanced Materials, Tohoku University, Sendai 980-8577, Japan*

(Dated: February 26, 2025)

[a] wakabayashi@tohoku.ac.jp

Abstract

Local polarization and charge transfer at the interface between 7-unit cell-thick $LaMnO_3$ (LMO) ultrathin films and substrates composed of Nb-doped (0.05 wt%) and undoped $SrTiO_3$ (STO) are examined by resonant surface x-ray diffraction. Notably, this photon-in photon-out technique allows us to simultaneously examine the valence distribution and local polarization with minimal radiation damage. Consistent with previous reports, Mn^{2+} is observed at the interface. Furthermore, the degree of charge transfer is nearly unchanged by the 0.05 wt% of Nb doping. In the middle of the LMO films, the valence of Mn is 3+. Local polarization estimated from the cation/anion displacements shows that the electric field points outward in the LMO films, and polarization is suppressed in the STO substrate region.

I. INTRODUCTION

Spontaneous charge transfer across the interfaces of metal oxides often plays a decisive role in their functionality[1–6]. Thus, the valence distribution around the interface has previously been investigated by applying cross-sectional transmission electron microscopy (TEM) in combination with electron energy-loss spectroscopy (EELS)[2, 7]. However, sample damage caused by sample preparation or electron beam irradiation may cause some uncertainty in the TEM-EELS measurements. For example, Mn^{2+} found at the interface between $LaMnO_3$ (LMO) and $LaNiO_3$ (LNO) was attributed to sample damage in ref.2, whereas the Mn^{2+} found by x-ray absorption spectroscopy (XAS) at the interface between LMO and $SrTiO_3$ (STO)[8] or at the surface[9] was regarded as intrinsic. Photon-in photon-out methods, such as XAS, are less invasive than those using electron beams, making x-ray spectroscopic probes more suitable for observing valence states. Nevertheless, it remains difficult to achieve atomic spatial resolution for XAS. The interfacial effects on the valence distribution can be localized to the interface in a few angstroms[7], and therefore, a less invasive probe that also has an Å-scale spatial resolution is desired for examining the valence condition.

Notably, surface x-ray diffraction provides detailed information on the surface/interface structures[10–12], and its spatial resolution allows us to observe local electric polarization[13, 14]. When we consider the absorption edge, this technique reveals not only the elemental arrangement[15, 16] but also the valence of ions[17–19]. By leveraging this technique, we examined the self-doping effect proposed at LMO/STO interfaces.

The charge, spin, and orbital (or lattice) degrees of freedom are intertwined in perovskite Mn oxides[20]. Furthermore, the magnetic properties of thick LMO/STO films have been examined as a function of the c-lattice spacing[8, 21–24]. Based on these studies, LMO/STO samples with a c-lattice spacing shorter than 3.94 Å ($= c_{\mathrm{FM}}$) exhibit ferromagnetic insulator behavior, whereas those with spacing longer than 3.97 Å exhibit bulk-like antiferromagnetic insulator behavior, and the lattice spacing depends on the annealing conditions. In ultrathin films, LMO/STO displays thickness-dependent magnetism[4], which may be determined by the electron transfer from the surface to the interface[4, 25–28]. It was also suggested that lattice strain plays a significant role in charge transfer at the interface[27]. Therefore, atomic resolution of the valence state is required to examine charge transfer phenomena at oxide interfaces.

In this study, we experimentally observed the valence arrangement across the LMO/STO interface, as well as the local polarization, ion concentration, and fluctuation of atomic positions. We examined two types of samples, namely ultrathin LMO films grown on STO and Nb-doped STO substrates. The samples were evaluated by employing the crystal truncation rod (CTR) scattering technique, which is a form of surface x-ray diffraction, utilizing the anomalous dispersion effect around the Mn K-absorption edge. We found that the structures of the two samples are nearly identical, and Mn^{2+}, which is not usually found in bulk Mn oxides, was found only at the interfaces.

II. EXPERIMENT AND ANALYSIS METHOD

Seven-unit cell-thick epitaxial LMO films were fabricated on atomically flat TiO_2-terminated STO and 0.05 wt% Nb:STO (001) substrates by pulsed laser deposition (PLD), denoted as $(LMO)_7$/STO and $(LMO)_7$/Nb:STO, respectively. First, the substrates were annealed at 1050°C under an oxygen pressure of 1×10^{-7} Torr to obtain atomically flat and chemically clean surfaces. During LMO deposition, the substrate was kept at 600°C, and the oxygen pressure was maintained at 1×10^{-3} Torr. A Nd-doped yttrium-aluminum-garnet laser in the frequency-triplet mode ($\lambda = 355$ nm) was used for ablation. The repetition rate and laser power were set to 1 Hz and 60-75 mJ, respectively. The thickness of the LMO layers was precisely controlled during growth by monitoring the intensity oscillation of the specular spot obtained under reflection high-energy electron diffraction. The LMO films

were subsequently annealed at 400°C for 45 min under an atmospheric pressure of oxygen to fill residual oxygen vacancies.

CTR scattering measurements were performed using the BL-3A beamline at the Photon Factory in Japan. The incident beam was linearly polarized perpendicular to the scattering plane. The scattered x-ray intensity was measured using a two-dimensional pixel array detector (XPAD-S70, imXpad, France). Samples were placed in a 10^{-5} Torr vacuum chamber to protect them from potential radiation damage, and all the measurements were performed at room temperature. Using 12 keV x-rays, a non-resonant condition, several $hk\zeta$ rods were measured up to $\zeta = 4.1$. Measurements along the 00ζ rod were also performed using the Mn K-absorption edge to discriminate the Mn valences. For measurements close to Mn K-edge, the polarization vector was parallel to [100] of the substrate.

After the measurements, illumination area correction and Lorentz factor correction were made by following the procedure described in ref. 29. The $hk\zeta$ intensity profiles along the rods were measured under both non-resonant and resonant conditions and simultaneously analyzed using exchange Monte-Carlo (MC) sampling software based on the Bayesian inference, CTR-structure code[30, 31]. In our analysis, the in-plane atomic positions were fixed to the simple cubic STO structure. Other parameters (i.e., atomic displacement in the surface normal direction (dz) with respect to the substrate lattice, atomic occupancy (occ), and isotropic atomic displacement parameter (B)) were refined. The total atomic occupancy for each site was set to unity, except for the surface region. The parameter uncertainty was estimated by MC sampling, accounting for the effective number of observations[31].

The spatial distribution of the Mn valence was derived from the (00ζ) CTR profiles measured at various x-ray energies. The energy spectrum obtained at a certain scattering vector depends on the non-resonant scattering amplitude, as well as the spatial arrangement of the Mn valence. Although the non-resonant amplitude was calculated based on the result of the interfacial structure analysis described above, it inevitably involves some error. The error was corrected by adding a small complex value as a function of the scattering vector, $C(\vec{Q})$, to the non-resonant scattering amplitude; this correction was also used in ref. 32. The anomalous scattering factors f' and f'' were calculated as functions of E for Mn^{3+} using FDMNES code[33] and the bulk $LaMnO_3$ structure[34]. The anomalous scattering factors for Mn^{2+} and Mn^{4+} were obtained by applying chemical shifts of -3 eV and 4 eV to those obtained for Mn^{3+}[35, 36]. The anomalous scattering factors are also sensitive to Jahn-

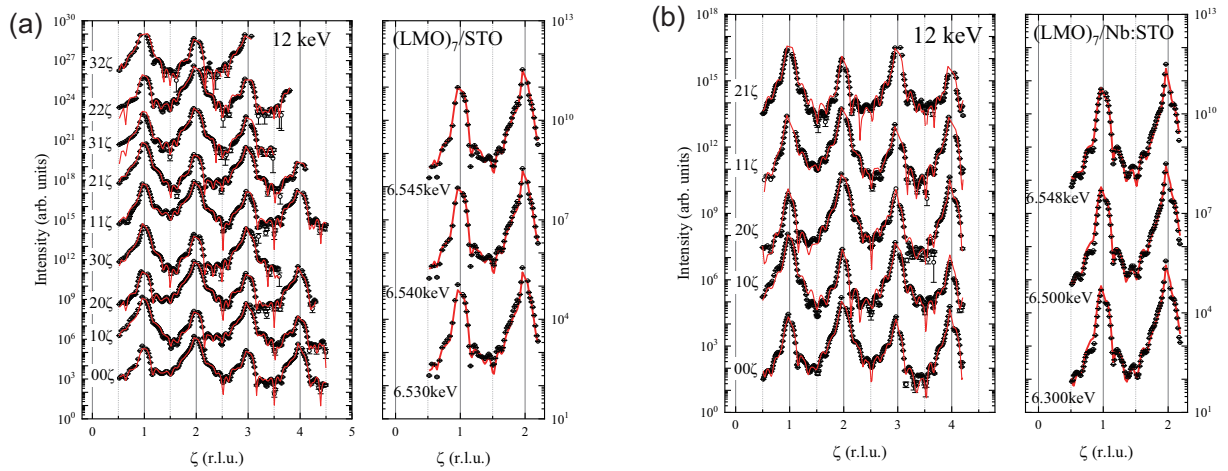

FIG. 1. CTR scattering intensity profiles for (a) $(LMO)_7$/STO and (b) $(LMO)_7$/Nb:STO measured at (left) 12 keV and the (right) Mn K-edge. Red curves show the fitting results.

Teller mode distortion[32] or shift of the Mn ion from the center of oxygen octahedron; we did not take such effects into account as the anisotropic effect is in-plane averaged when we think about 00ζ-rod. The analysis was also performed considering the Bayesian inference, assuming that the magnitude of the noise was 10 % of the intensity. The error bars of the Mn^{4+} concentration were estimated by MC sampling, whereas the effective number of observations for the energy spectra was assumed to be the same as the number of data points.

III. RESULTS AND DISCUSSION

The non-resonant and resonant CTR profiles for $(LMO)_7$/STO and $(LMO)_7$/Nb:STO films are presented in Fig. 1. Here, R ($\equiv \sum_{\zeta,E}[|(|F_{\rm expt}| - |F_{\rm calc}|)|]/[\sum_{\zeta,E}|F_{\rm expt}|]$, where $F_{\rm expt}$ and $F_{\rm calc}$ denote the square root of the measured and calculated intensity) was 0.11 and 0.13 for $(LMO)_7$/STO and $(LMO)_7$/Nb:STO, respectively, which are ordinary values for CTR analysis[19, 37]. The resulting structural parameters for each site are shown in Fig. 2 as functions of the depth, z. The position of $z = 0$ corresponds to the interface, and the surface is located at $z \simeq 7$ for the two samples.

Figure 2 shows that there is little difference in structure between the $(LMO)_7$/STO and $(LMO)_7$/Nb:STO samples, especially in the depth dependence of the elemental occupancy

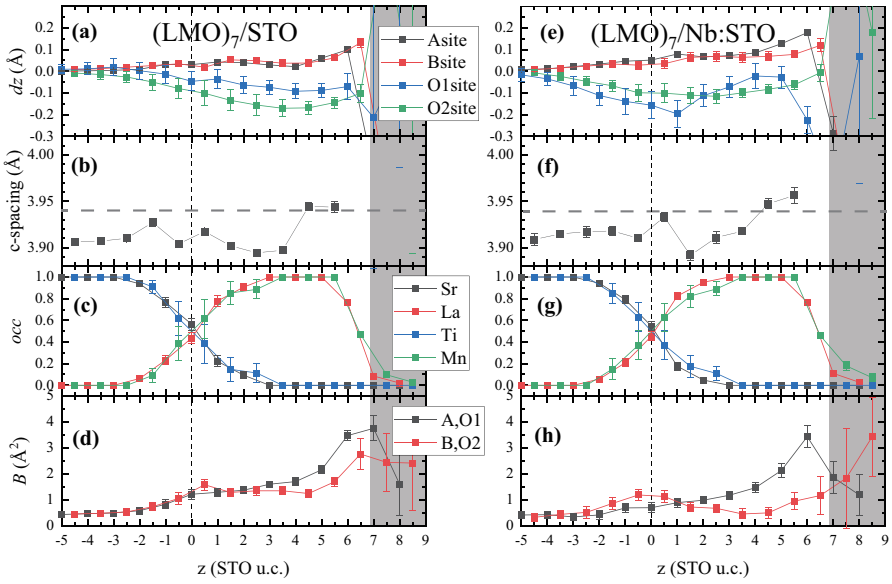

FIG. 2. Depth dependence of the obtained structure parameters for (a-d) $(LMO)_7$/STO and (e-h) $(LMO)_7$/Nb:STO. The origin of the horizontal axis is set as the interface. (a,e) Atomic displacement with respect to the substrate lattice, (b, f) c-lattice spacing defined by the inter-A-site distance, (c,g) occupancy, and (d,h) isotropic atomic displacement parameter B. Atomic occupancies and the B parameters of the oxygen atoms are assumed to be the same as those of the cation in the same z layer. The shaded areas indicate the regions with small occupancy parameters, where the reliability of all other parameters is poor. The horizontal dashed lines in panels (b) and (f) show the c_{FM}.

presented in panels (c) and (g). This demonstrates the reproducibility of the film growth. The transient regions of the occupancy at the interfaces are thicker than those at the surfaces, meaning that the LMO/STO interface contains a significant amount of atomic interdiffusion. Conversely, the transient regions at the LNO/$LaAlO_3$ (LAO) interface have similar thicknesses to those at their surfaces [37]. This discrepancy may be attributed to the large diffusion constant of Sr[38] or the polar discontinuity. Another possible explanation for the thicker transient region in the present samples is that the PLD process produces a flatter surface than the substrate. The atomic displacement parameters B are $\sim$0.5 Å^2 in the substrate lattice, $\sim$ 1.5 Å^2 at the interface, and less than 2 Å^2 in most of the film, as shown in panels (d) and (h). These values are similar to LNO/LAO[37] and LNO/LMO bilayers on STO substrates[19]. Slightly enhanced B values in the film region appear to be common

characteristics in epitaxial oxide films.

The local polarization can be examined based on the atomic displacements presented in Fig. 2(a) and (e). In this study, the atomic displacement along the c direction is examined, thus the c component of the polarization can be discussed. The cations are always located above oxygen atoms, meaning that the electric field in this material points outwards, which is consistent with the theoretical expectation for lattices containing few vacancies[8, 9]. The polarization distribution in LMO/STO suggests moderate charge distribution in LMO region. Charges are distributed mainly in STO side and on the surface. The polarization direction does not change at the interface, which exhibits a contrast with the polarization direction change at LNO/LMO interface[19]. Such a local polarization suggests that electric flux diverges from the space charge layer in the STO, and converges into the negatively charged contamination outside of the film. The polarization distribution is also different from 2D-electron gas system LAO/STO[14], in which the electric flux diverges from the space charge layer in the STO and converges to the interface. Since LAO/STO and LMO/STO are both polar/nonpolar interfaces, the difference in the polarization distribution is caused by the different band gap and band alignment between the two interfaces.

The c-lattice spacing is defined by the distance between the A-site ions, and thus the value represents the available space for the central Mn ion. The depth profiles are presented in Fig. 2(b) and (f). Deep inside the substrate, the value is the same as that of the bulk STO lattice parameter, 3.905 Å. The c-lattice spacings of the films were 3.91±0.01Å in the $z < 5$ region, which are shorter than c_{FM}. The spacing is increased at the surface; surface expansion is also observed in $La_{1-x}Sr_xMnO_3$ films on STO[38, 39], whereas no such characteristic was reported for LNO/LAO[37, 40], LNO/STO[41], or LAO/STO[13, 14, 42, 43]. Herein, the c-lattice spacings expanded to 3.95±0.01Å near the surface, in the range of $5 \leq z < 7$. Therefore, most of the LMO film is expected to be ferromagnetic, and only the surface region can be antiferromagnetic. The c-lattice spacing can also be used as a measure of the Mn valence. The c-lattice spacing and the hole concentration (x) dependence of the c-lattice spacing for $LaMn^{3+}O_3$ grown on STO were estimated as $c = 3.973$ Å and dc/dx=−0.34 Å[19], respectively. Using these values, the valences of Mn ions at $c = 3.90$ Å and 3.94 Å ($= c_{\mathrm{FM}}$) are estimated to be 3.21+ and 3.10+. This estimation can be used only in the middle of the LMO layer, where the occupancy of the La, Mn, and O are supposed to be 1.

To examine the valence arrangement at the interface, many energy spectra were measured

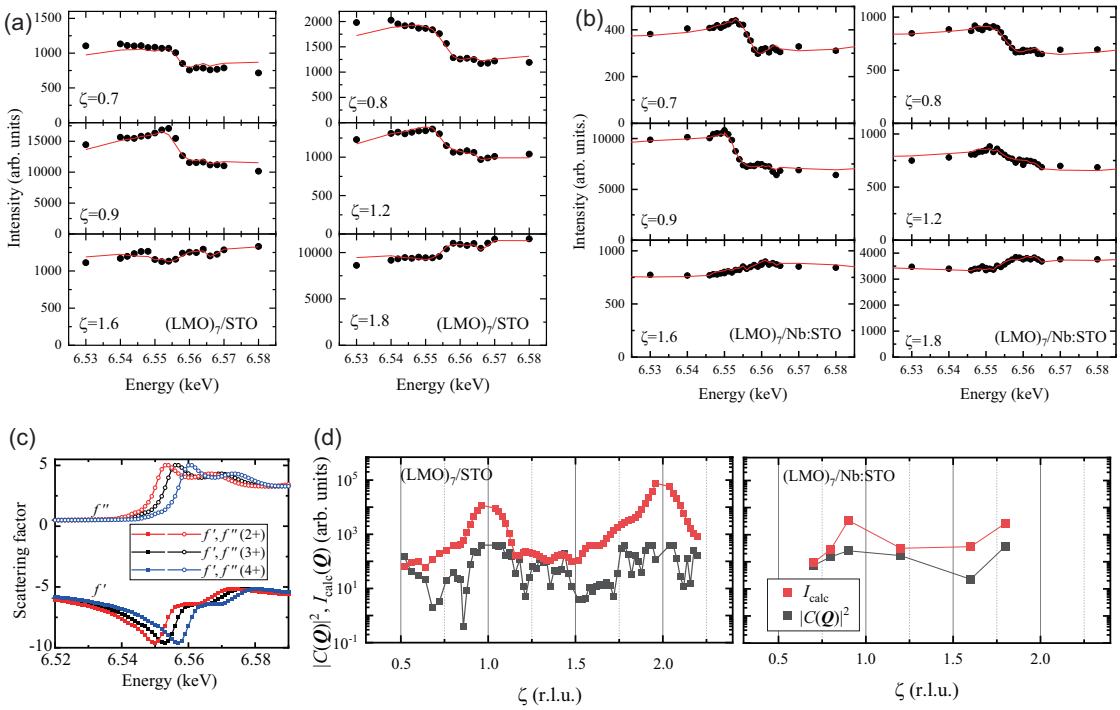

FIG. 3. Energy spectra at several (00ζ) positions around the Mn K-edge for (a) $(LMO)_7$/STO and (b) $(LMO)_7$/Nb:STO. Red curves show the fitting results. (c) Anomalous scattering factors for Mn^{2+}, Mn^{3+}, and Mn^{4+}. (d) Calculated intensity and modulus square of the correction term $C(\zeta)$.

over the Mn K-edge on the 00ζ-rod, as shown in Fig. 3. The energy spectra measurements slightly differed for the two samples. For $(LMO)_7$/STO, we measured numerous (00ζ) profiles at various x-ray energies, and for $(LMO)_7$/Nb:STO, we measured energy spectra at several (00ζ) positions, resulting in a different number of data points for the ζ profiles (denser in $(LMO)_7$/STO) and energy spectra (denser in $(LMO)_7$/Nb:STO). The red plots in Fig. 3(d) show the calculated intensity $I_{calc}(\vec{Q})$, and the black plots show the modulus square of the correction term $C(\vec{Q})$. The analysis shows that I_{calc} is always greater than $|C(\vec{Q})|^2$, and in most cases, the correction term is found to be minor, showing that the error in our structure model is minimal.

The derived valence distributions of Mn ions for the two samples are shown in Fig. 4. Most of the Mn ions are close to Mn^{3+}, as expected. Panels (a) and (c) show the occupancy of divalent, trivalent, and tetravalent Mn derived from our MC analysis. The only information

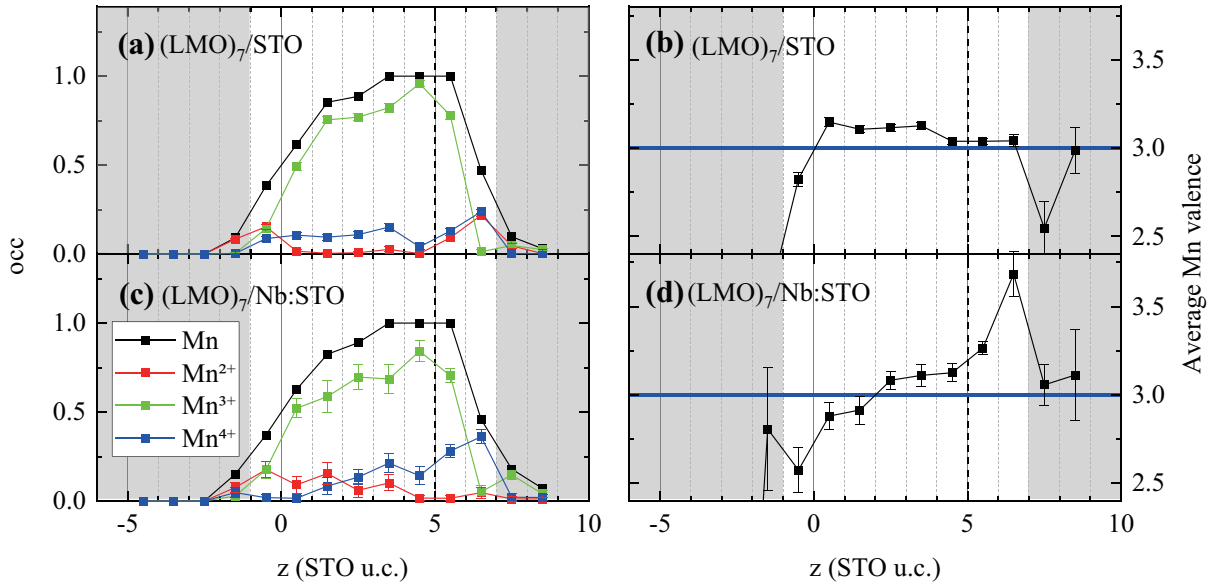

FIG. 4. Depth profiles of (a) the occupancy parameters for Mn, Mn^{2+}, Mn^{3+} and Mn^{4+} and (b) the average Mn valence for $(LMO)_7$/STO. (c), (d) show those for $(LMO)_7$/Nb:STO.

that affects the energy spectra of the intensity is the averaged anomalous scattering factor $\overline{f} = \sum_n [f'(n+) + if''(n+)]occ(n+)$ for each Mn site, and $\overline{f}$ is only sensitive to the average Mn valence. The average valences of Mn at $z = 4.5$, where the occupancy of Mn is unity, for the two samples are 3.04+ and 3.12+, as shown in panels (b) and (d). These values are similar to those estimated from the c-lattice spacing. At the surface, the average valence of Mn was 3.04(3)+ for $(LMO)_7$/STO and 3.68(13)+ for$(LMO)_7$/Nb:STO, but it is unclear whether the surface valence has been affected by contamination, given that the samples were handled in air. At the interface, both samples contain Mn^{2+}. Note that Mn^{2+} is found where the occupancy of Mn is significantly reduced from 1. Although Sr diffusion should cause Mn^{4+} accumulation at the interface, Mn^{2+} is found, which is consistent with the electronic potentials calculated for the ideal interfacial structure[8, 9].

IV. CONCLUSION

We performed surface/interface structure analyses based on surface x-ray diffraction and obtained energy spectra of the surface diffraction intensity for LMO/STO and LMO/Nb:STO interfaces. The structural information was derived from the non-resonant scattering inten-

sity, and the electric field in the LMO region was oriented outward, consistent with a previous report[8]. Using the structural information and the energy spectra, we derived the Mn valence distribution. Mn^{2+} ions were only found at the interface, and the spatial distribution of Mn^{2+} was insensitive to the Nb doping of the STO substrate. Overall, the resonant CTR method is useful for simultaneously deriving the valence information and local polarization on the same sample with minimal sample damage.

ACKNOWLEDGMENTS

This work was supported by a Grant-in-Aid for Scientific Research [Japan Society for the Promotion of Science (JSPS) KAKENHI, Grant Nos. JP22H02024 and JP23K23292]. The synchrotron radiation experiments at the Photon Factory were performed with the approval of the Photon Factory Program Advisory Committee (Proposal No. 2018G533 and No. 2020G526). We thank Robert Ireland, PhD, from Edanz (https://jp.edanz.com/ac) for editing a draft of this manuscript.

[1] A. Ohtomo and H. Hwang, A high-mobility electron gas at the $LaAlO_3/SrTiO_3$ heterointerface, Nature **427**, 423 (2004).

[2] M. Gibert, M. Viret, A. Torres-Pardo, C. Piamonteze, P. Zubko, N. Jaouen, J.-M. Tonnerre, A. Mougin, J. Fowlie, S. Catalano, A. Gloter, O. Stéphan, and J.-M. Triscone, Interfacial Control of Magnetic Properties at $LaMnO_3/LaNiO_3$ Interfaces, Nano Lett. **15**, 7355 (2015).

[3] M. Huijben, Y. Liu, H. Boschker, V. Lauter, R. Egoavil, J. Verbeeck, S. G. Te Velthuis, G. Rijnders, and G. Koster, Enhanced local magnetization by interface engineering in perovskite-type correlated oxide heterostructures, Advanced Materials Interfaces **2**, 1400416 (2015).

[4] X. Wang, C. Li, W. Lü, T. Paudel, D. Leusink, M. Hoek, N. Poccia, A. Vailionis, T. Venkatesan, J. Coey, E. Tsymbal, Ariando, and H. Hilgenkamp, Imaging and control of ferromagnetism in $LaMnO_3/SrTiO_3$ heterostructures, Science **349**, 716 (2015).

[5] H. Hwang, Y. Iwasa, M. Kawasaki, B. Keimer, N. Nagaosa, and Y. Tokura, Emergent phenomena at oxide interfaces, Nature Materials **11**, 103 (2012).

[6] S. Middey, J. Chakhalian, P. Mahadevan, J. Freeland, A. Millis, and D. Sarma, Physics of ultrathin films and heterostructures of rare-earth nickelates, Annual Review of Materials Research **46**, 305 (2016).

[7] A. Ohtomo, D. Muller, J. Grazul, and H. Hwang, Artificial charge-modulation in atomic-scale perovskite titanate superlattices, Nature **419**, 378 (2002).

[8] Z. Chen, Z. Chen, Z. Q. Liu, M. E. Holtz, C. J. Li, X. R. Wang, W. M. Lü, M. Motapothula, L. S. Fan, J. A. Turcaud, L. R. Dedon, C. Frederick, R. J. Xu, R. Gao, A. T. N'Diaye, E. Arenholz, J. A. Mundy, T. Venkatesan, D. A. Muller, L.-W. Wang, J. Liu, and L. W. Martin, Electron Accumulation and Emergent Magnetism in $LaMnO_3/SrTiO_3$ Heterostructures, Phys. Rev. Lett. **119**, 156801 (2017).

[9] T. C. Kaspar, P. V. Sushko, S. R. Spurgeon, M. E. Bowden, D. J. Keavney, R. B. Comes, S. Saremi, L. Martin, and S. A. Chambers, Electronic Structure and Band Alignment of $LaMnO_3/SrTiO_3$ Polar/Nonpolar Heterojunctions, Advanced Materials Interfaces **6**, 1801428 (2019).

[10] I. K. Robinson, R. T. Tung, and R. Feidenhans'l, X-ray interference method for studying interface structures, Phys. Rev. B **38**, 3632 (1988).

[11] Y. Wakabayashi, T. Shirasawa, W. Voegeli, and T. Takahashi, Observation of Structure of Surfaces and Interfaces by Synchrotron X-ray Diffraction: Atomic-Scale Imaging and Time-Resolved Measurements, Journal of the Physical Society of Japan **87**, 061010 (2018).

[12] A. S. Disa, F. J. Walker, and C. H. Ahn, High-resolution crystal truncation rod scattering: Application to ultrathin layers and buried interfaces, Advanced Materials Interfaces **7**, 1901772 (2020).

[13] P. Willmott, S. Pauli, R. Herger, C. Schlepütz, D. Martoccia, B. Patterson, B. Delley, R. Clarke, D. Kumah, C. Cionca, and Y. Yacoby, Structural basis for the conducting interface between $LaAlO_3$ and $SrTiO_3$, Phys. Rev. Lett. **99**, 155502 (2007).

[14] R. Yamamoto, C. Bell, Y. Hikita, H. Hwang, H. Nakamura, T. Kimura, and Y. Wakabayashi, Structural comparison of n-type and p-type $LaAlO_3/SrTiO_3$ interfaces, Phys. Rev. Lett. **107**, 036104 (2011).

[15] E. Perret, C. Park, D. D. Fong, K.-C. Chang, B. J. Ingram, J. A. Eastman, P. M. Baldo, and P. H. Fuoss, Resonant X-ray scattering studies of epitaxial complex oxide thin films, J. Appl. Cryst. **46**, 76 (2013).

[16] Y. Joly, A. Abisset, A. Bailly, M. De Santis, F. Fettar, S. Grenier, D. Mannix, A. Y. Ramos, M.-C. Saint-Lager, Y. Soldo-Olivier, J.-M. Tonnerre, S. A. Guda, and Y. Gründer, Simulation of surface resonant x-ray diffraction, J. Chem. Theory Comput. **14**, 973 (2018).

[17] E. D. Specht and F. J. Walker, Oxidation state of a buried interface: Near-edge x-ray fine structure of a crystal truncation rod, Phys. Rev. B **47**, 13743 (1993).

[18] Y. S. Chu, H. You, J. A. Tanzer, T. E. Lister, and Z. Nagy, Surface Resonance X-Ray Scattering Observation of Core-Electron Binding-Energy Shifts of Pt(111)-Surface Atoms during Electrochemical Oxidation, Phys. Rev. Lett. **83**, 552 (1999).

[19] M. Anada, S. Sakaguchi, K. Nagai, M. Kitamura, K. Horiba, H. Kumigashira, and Y. Wakabayashi, Local polarization and valence distribution in $LaNiO_3/LaMnO_3$ heterostructures, Phys. Rev. B **104**, 085111 (2021).

[20] Y. Tokura and N. Nagaosa, Orbital physics in transition-metal oxides, Science **288**, 462 (2000).

[21] W. Choi, Z. Marton, S. Jang, S. Moon, B. Jeon, J. Shin, S. Seo, T. Noh, K. Myung-Whun, H. Lee, and Y. Lee, Effects of oxygen-reducing atmosphere annealing on $LaMnO_3$ epitaxial thin films, J. Phys. D: Appl. Phys. **42**, 165401 (2009).

[22] W. S. Choi, D. Jeong, S. Jang, Z. Marton, S. Seo, H. Lee, and Y. Lee, $LaMnO_3$ Thin Films Grown by Using Pulsed Laser Deposition and Their Simple Recovery to a Stoichiometric Phase by Annealing, J. Korean. Phys. Soc. **58**, 569 (2011).

[23] I. V. Borisenko, M. A. Karpov, and G. A. Ovsyannikov, Metal-insulator transition in epitaxial films of $LaMnO_3$ manganites grown by magnetron sputtering, Tech. Phys. Lett **39**, 1027 (2013).

[24] J. Roqueta, A. Pomar, L. Balcells, C. Frontera, S. Valencia, R. Abrudan, B. Bozzo, Z. Konstantinović, J. Santiso, and B. Martínez, Strain-Engineered Ferromagnetism in $LaMnO_3$ Thin Films, Cryst. Growth Des. **15**, 5332 (2015).

[25] X. Zhai, C. S. Mohapatra, A. B. Shah, J.-M. Zuo, and J. N. Eckstein, Magnetic properties of the $(LaMnO_3)_N/(SrTiO_3)_N$ atomic layer superlattices, J. Appl. Phys. **113**, 173913 (2013).

[26] W. S. Choi, D. W. Jeong, S. S. A. Seo, Y. S. Lee, T. H. Kim, S. Y. Jang, H. N. Lee, and K. Myung-Whun, Charge states and magnetic ordering in $lamno_3/srtio_3$ superlattices, Phys. Rev. B **83**, 195113 (2011).

[27] J. Garcia-Barriocanal, F. Y. Bruno, A. Rivera-Calzada, Z. Sefrioui, N. M. Nemes, M. Garcia-Hernández, J. Rubio-Zuazo, G. R. Castro, M. Varela, S. J. Pennycook, C. Leon, and J. San-

tamaria, Charge Leakage at $LaMnO_3/SrTiO_3$ Interfaces, Adv. Mater. **22**, 627 (2010).

[28] J. Garcia-Barriocanal, J. C. Cezar, F. Y. Bruno, P. Thakur, N. B. Brookes, C. Utfeld, A. Rivera-Calzada, S. R. Giblin, J. W. Taylor, J. A. Duffy, S. B. Dugdale, T. Nakamura, K. Kodama, C. Leon, S. Okamoto, and J. Santamaria, Spin and orbital Ti magnetism at $LaMnO_3/SrTiO_3$ interfaces, Nat. Commun. **1**, 82 (2010).

[29] C. M. Schlepütz, R. Herger, P. R. Willmott, B. D. Patterson, O. Bunk, C. Brönnimann, B. Henrich, G. Hülsen, and E. F. Eikenberry, Improved data acquisition in grazing-incidence X-ray scattering experiments using a pixel detector, Acta Cryst. A **61**, 418 (2005).

[30] M. Anada, Y. Nakanishi-Ohno, M. Okada, T. Kimura, and Y. Wakabayashi, Bayesian inference of metal oxide ultrathin film structure based on crystal truncation rod measurements, J. Appl. Cryst. **50**, 1611 (2017).

[31] K. Nagai, M. Anada, Y. Nakanishi-Ohno, M. Okada, and Y. Wakabayashi, Robust surface structure analysis with reliable uncertainty estimation using the exchange monte carlo method, J. Appl. Cryst. **53**, 387 (2020).

[32] Y. Wakabayashi, H. Sawa, M. Nakamura, M. Izumi, and K. Miyano, Lack of influence of anisotropic electron clouds on resonant x-ray scattering from manganite thin films, Phys. Rev. B **69**, 144414 (2004).

[33] O. Bunău and Y. Joly, Self-consistent aspects of x-ray absorption calculations, J. Phys.: Condens. Matter **21**, 345501 (2009).

[34] J. Rodríguez-Carvajal, M. Hennion, F. Moussa, A. H. Moudden, L. Pinsard, and A. Revcolevschi, Neutron-diffraction study of the Jahn-Teller transition in stoichiometric $LaMnO_3$, Phys. Rev. B **57**, 3189 (1998).

[35] H. Nakao, J. Nishimura, Y. Murakami, A. Ohtomo, T. Fukumura, M. Kawasaki, T. Koida, Y. Wakabayashi, and H. Sawa, Crystal Structure and Valence Distribution of $[(LaMnO_3)_m(SrMnO_3)_m]_n$ Artificial Superlattices, J. Phys. Soc. Jpn. **78**, 024602 (2009).

[36] G. Subías, J. García, M. G. Proietti, and J. Blasco, X-ray-absorption near-edge spectroscopy and circular magnetic x-ray dichroism at the Mn K edge of magnetoresistive manganites, Phys. Rev. B **56**, 8183 (1997).

[37] K. Nagai, M. Anada, K. Kowa, M. Kitamura, H. Kumigashira, H. Tajiri, and Y. Wakabayashi, Quantitative Measurement of Structural Fluctuation at the Metallic and Insulating Interfaces between $LaNiO_3$ and $LaAlO_3$, Phys. Rev. Mater. **7**, 043604 (2023).

[38] R. Herger, P. R. Willmott, C. M. Schlepütz, M. Björck, S. A. Pauli, D. Martoccia, B. D. Patterson, D. Kumah, R. Clarke, Y. Yacoby, and M. Döbeli, Structure determination of monolayer-by-monolayer grown $La_{1-x}Sr_xMnO_3$ thin films and the onset of magnetoresistance, Phys. Rev. B **77**, 085401 (2008).

[39] S. Koohfar, A. S. Disa, M. S. J. Marshall, F. J. Walker, C. H. Ahn, and D. P. Kumah, Structural distortions at polar manganite interfaces, Phys. Rev. B **96**, 024108 (2017).

[40] D. P. Kumah, A. Malashevich, A. S. Disa, D. A. Arena, F. J. Walker, S. Ismail-Beigi, and C. H. Ahn, Effect of Surface Termination on the Electronic Properties of $LaNiO_3$ Films, Phys. Rev. Applied **2**, 054004 (2014).

[41] I.-C. Tung, G. Luo, J. H. Lee, S. H. Chang, J. Moyer, H. Hong, M. J. Bedzyk, H. Zhou, D. Morgan, D. D. Fong, and J. W. Freeland, Polarity-driven oxygen vacancy formation in ultrathin $LaNiO_3$ films on $SrTiO_3$, Phys. Rev. Materials **1**, 053404 (2017).

[42] S. A. Pauli, S. J. Leake, B. Delley, M. Björck, C. W. Schneider, C. M. Schlepütz, D. Martoccia, S. Paetel, J. Mannhart, and P. R. Willmott, Evolution of the Interfacial Structure of $LaAlO_3$ on $SrTiO_3$, Phys. Rev. Lett. **106**, 036101 (2011).

[43] T. Fister, H. Zhou, Z. Luo, S. Seo, S. Hruszkewycz, D. Proffit, J. Eastman, P. Fuoss, P. Baldo, H. Lee, and D. Fong, Octahedral rotations in strained $LaAlO_3/SrTiO_3$ (001) heterostructures, APL Materials **2**, 021102 (2014).